Journal for ImmunoTherapy of Cancer

Mapping B cells and the immune landscape of tertiary lymphoid structures reveals their clinical impact in neuroblastoma

Ombretta Melaiu,[1,2] Marco Chierici,[3] Paula Gragera,[1] Nicolò Lazzaro,[3] Lucia L Petrilli,[1] Judith Wienke,[4] Francisca J Bergsma,[4] Bronte Manouk Verhoeven,[5] Cristiano De Stefanis,[1] Valentina D'Oria,[1] Maria C Benedetti,[1] Giovanni Barillari,[2] Rita Alaggio,[1] Maria Antonietta De Ioris,[1] Maria Vinci,[1] Ninib Baryawno,[5] Rita Carsetti,[1] Giuseppe Jurman,[3,6] Jan J Molenaar,[4] Franco Locatelli,[1,7] Doriana Fruci [1]

To cite: Melaiu O, Chierici M, Gragera P, *et al*. Mapping B cells and the immune landscape of tertiary lymphoid structures reveals their clinical impact in neuroblastoma. *Journal for ImmunoTherapy of Cancer* 2025;**13**:e012860. doi:10.1136/jitc-2025-012860

► Additional supplemental material is published online only. To view, please visit the journal online (https://doi.org/10.1136/jitc-2025-012860).

MC and PG contributed equally.

Accepted 21 October 2025

For numbered affiliations see end of article.

Correspondence to
Dr Doriana Fruci;
doriana.fruci@opbg.net

ABSTRACT

Background Immunotherapy has transformed cancer treatment, highlighting the importance of effective antitumor immunity to fight cancer. However, its success in pediatric cancer remains limited, underscoring the urgent need to identify new immunotherapeutic targets. In this study, we explored the clinical relevance of B cells and tertiary lymphoid structures (TLS) in neuroblastoma (NB), a pediatric tumor with a heterogeneous immune landscape.

Methods We analyzed 87 treatment-naïve NB specimens, spanning both localized and metastatic disease previously characterized for T-cell and dendritic cell (DC) infiltration. B cells were detected by immunohistochemistry, and plasma cells were quantified using multiple immunofluorescence. Spatial organization and functional status of immune cells within TLSs were assessed by imaging mass cytometry using a 29-antibody panel. In parallel, gene expression profiles were obtained through NanoString PanCancer Immune Profiling and further validated using publicly available bulk and single-cell RNA-sequencing data from untreated and treated NB samples. These transcriptomic datasets were used to support protein-level findings and to identify prognostic gene signatures.

Results B-cell infiltration in NB tumors strongly correlated with the presence of T cells and DCs at both protein and transcriptomic levels, and was associated with improved prognosis. Similar to other solid tumors, B cells in NB were either scattered throughout the tumor or organized into TLSs of varying maturity. Spatial proteomic and transcriptomic analyses revealed that localized tumors often contain mature TLSs, with functional B cells able to antigen presentation and immunoglobulin expression, alongside high cytotoxic T cells. In contrast, metastatic tumors primarily exhibited immature TLSs, with evidence of B-cell and T-cell dysfunction. Importantly, we identified gene signatures associated with B cells and TLSs that not only predicted survival in NB but were also prognostic in multiple adult cancers.

Conclusions Our findings highlight a central role for B cells and TLSs in shaping the immune microenvironment of NB. Their presence and maturation status are linked to clinical outcome, suggesting their potential as prognostic biomarkers and targets for novel immunotherapeutic strategies in pediatric oncology.

WHAT IS ALREADY KNOWN ON THIS TOPIC

⇒ Immunotherapy has transformed cancer treatment by enhancing antitumor immunity, but its benefits in pediatric cancers such as neuroblastoma (NB) remain limited. Previous studies have demonstrated that tumor-infiltrating T cells, dendritic cells (DC), and natural killer cells are associated with improved clinical outcomes in NB. However, the role of B cells and tertiary lymphoid structures (TLSs) in NB's immune microenvironment and their clinical relevance had not been fully explored.

WHAT THIS STUDY ADDS

⇒ This study reveals that B-cell infiltration and the presence of TLSs correlate positively with T-cell and DC infiltration and are linked to better prognosis in patients with NB. We provide evidence that localized NB tumors contain mature TLSs with activated B cells capable of antigen presentation and strong cytotoxic T-cell responses, whereas metastatic tumors primarily harbor immature TLSs with dysfunctional immune cells. Importantly, we identified novel gene signatures related to B cells and TLSs that predict patient survival in NB and other adult cancers, representing new prognostic markers.

HOW THIS STUDY MIGHT AFFECT RESEARCH, PRACTICE OR POLICY

⇒ Our findings highlight the critical role of B cells and TLS maturation in shaping NB's immune landscape, suggesting their potential as prognostic biomarkers and targets for novel immunotherapeutic strategies in pediatric oncology. This work supports more personalized approaches to immunotherapy by identifying patients likely to benefit from current and future treatments, and may guide the development of B cell- and TLS-focused therapies in NB.

BACKGROUND

Immune checkpoint inhibitors (ICIs) have revolutionized adult cancer treatment, but their efficacy in pediatric tumors remains limited, mainly due to lower tumor immunogenicity.[1] A deeper understanding of the tumor immune microenvironment (TIME) in pediatric tumors is essential to identify new immunotherapeutic targets and predictive biomarkers.

Neuroblastoma (NB), the most common extracranial solid tumor in children and responsible for 10% of childhood cancer-related deaths despite intensive therapy,[2] offers a unique model to address immunotherapy challenges.[3] This is due to (1) its high rate of spontaneous regression, likely driven by immune activation,[2] and (2) encouraging preclinical results showing enhanced immunotherapy responses in aggressive NB models.[4 5] We previously demonstrated that high $CD8^+$ T-cell infiltration correlates with better prognosis in patients with NB.[6] However, a T-cell-centric view does not fully explain the prognostic and predictive significance of tumor-infiltrating lymphocytes (TILs). We observed that T cell-rich NB samples also contain abundant dendritic cells (DC) and natural killer (NK) cells, associated with greater cytotoxic T-cell activity and increased expression of programmed cell death protein-1 (PD-1) and programmed death-ligand 1 (PD-L1).[7 8] Notably, DCs in localized NBs frequently cluster with T cells and other lymphocytes than NK cells.[7]

Tumor-infiltrating B cells retain active immune functions, such as antigen recognition, clonal expansion, phenotypic differentiation, and production of hypermutated antitumor antibodies.[9–11] Consistently, B cells have demonstrated prognostic value in various adult malignancies and are involved in response to ICIs.[12 13] Within the TIME, B cells interact with other immune cells in structures ranging from lympho-myeloid aggregates to more organized tertiary lymphoid structures (TLSs).[14 15] TLSs develop at sites of inflammation and resemble the secondary lymphoid organs, comprising central $CD20^+$ B cells, surrounded by DCs and a T-cell mantle including $CD4^+$, $CD8^+$ T cells and regulatory T cells (Treg).[16] TLSs have been identified in several adult solid tumors, where their presence often correlates with better prognosis and improved responses to ICIs.[17–20] However, their prognostic role in NB remains unexplored.

In this study, we addressed the clinical relevance of tumor-infiltrating B cells and TLSs in NB. We show that their presence correlates with favorable prognosis and enhanced T-cell cytotoxicity. Using single-cell RNA sequencing (scRNA-seq) and spatial proteomics, we demonstrate that localized NBs harbor mature TLSs that support efficient antibody response, mediated by antigen-presenting B cells, plasma cells, and functional $CD8^+$ T cells. Additionally, through our NanoString and public RNA-seq datasets, we identified two gene signatures, one for B cells and one for TLSs, that strongly predict the survival in patients with NB, and validated them across multiple adult cancer types.

METHODS

Patients and samples

A total of 87 patients with NB diagnosed between 2002 and 2017 at the Bambino Gesù Children's Hospital (Rome, Italy) were enrolled. Samples were collected at diagnosis, prior to any therapy. Frozen material was available for 36 patients for gene expression. Clinical data are summarized in online supplemental table S1. Diagnosis and tumor classification were performed according to INRG, INSS and INPC systems.[21] MYCN amplification and chromosome 1p deletion were evaluated following established protocols.[22] Patients received standard risk-adapted protocols.[23–26] The samples were classified according to the INRG system as follows: stage L1 includes locoregional tumors without image-defined risk factors (IDRFs); stage L2 includes locoregional tumors with one or more IDRFs; stage M refers to tumors with distant metastases (excluding MS); and stage MS denotes L1 or L2 tumors with metastases confined to the skin, liver, and/or bone marrow.

Antibodies for immunostaining

Antibodies used for immunohistochemistry (IHC) and immunofluorescence (IF) staining optimized on normal tonsils, are listed in online supplemental table S2. Isotype-matched mouse monoclonal antibodies were used as negative controls.

Immunohistochemistry and acquisition

Formalin-fixed paraffin-embedded (FFPE) sections (2 µm) were deparaffinized and pretreated in PT-Link (DAKO) with pH 6 target retrieval buffer. After peroxidase blocking (5 min), sections were incubated overnight at 4°C with primary antibodies. EnVision HRP-labeled polymer and 3,3'-diaminobenzidine (DAB) substrate were used for detection. Slides were counterstained with hematoxylin, dehydrated, mounted, and scanned using a NanoZoomer S60 scanner. The immune cell density was determined by two blinded examiners as positive cells/mm^2 normalized to tumor cellularity (ranging from 400 to 700 cells per field). The average density from 10 fields/sample was log-transformed using ln (x+1/(1+x)) for statistical analysis.

Double immunofluorescence

FFPE sections (2 µm) were deparaffinized, antigen retrieved (pH 6),[6–8] blocked with 1% Bovine Serum Albumin (BSA)/5% goat serum and incubated with anti-CD20 antibody overnight. After secondary antibody incubation (Alexa Fluor-594 goat anti-mouse IgG, 1 hour) anti-CD138 antibody was applied overnight followed by Alexa Fluor Plus 647 Donkey anti-Rat-IgG. Hoechst was used for nuclear staining. Confocal imaging was performed with a Leica TCS-SP8X laser-scanning confocal microscope (Leica Microsystems) using 40× oil immersion objective $CD20^-CD138^+$ plasma cells were counted in five fields/sample.

Antibody optimization and imaging mass cytometry

Ten NB samples with TLSs were selected, covering all INRG stages (4 L1, 3 L2 and 3 M). A 29-antibody panel (online supplemental table S3) was used, with 18 commercial antibodies and others conjugated using Maxpar X8 Labeling Kits. Antibodies were validated on control tissues (tonsil, colon cancer) by IHC. Conjugated antibodies were stored in phosphate-buffered saline 2^{+} (0.05% NaN3).

Tissue labeling and imaging mass cytometry acquisition

FFPE sections were deparaffinized, antigen retrieved (Tris/EDTA pH 9.0) and blocked with 2% BSA. Slides were incubated with the antibody panel overnight at 4°C, followed by iridium DNA staining (0.5 µM, 30 min). After washing, 10 TLS-containing regions of interest (ROIs) (850×850 μm^2) per sample were selected from H&E scanned slides. Imaging mass cytometry (IMC) was performed with the Hyperion system (Standard BioTools), ablating tissue at 1 µm resolution and quantifying isotypes via time-of-flight mass spectrometry.

Imaging mass cytometry data analysis

IMC image analysis of raw data (.mcd files) was performed using the Steinbock toolkit (V.0.16.1) and analysis pipeline previously reported by Windhager *et al*.[27] Detailed information on data analysis is reported on online supplemental material.

NanoString gene expression profiling

36 NB samples (online supplemental file 22) were analyzed using the NanoString PanCancer Immune Profiling Panel (730 immune-related+40 housekeeping genes), as previously described.[7] RNA was extracted with the Total RNA Purification Plus kit (Norgen, Biotek Thorold) and purified with RNA Cleanup and Concentration kit (Norgen, Biotek Thorold). Integrity was confirmed by Bioanalyzer kit (Agilent Technologies) and quantified with NanoDrop. Data were normalized and processed per NanoString guidelines.[7] Genes were grouped into 11 immune cell type signatures (cytotoxic and helper T cells, DC, NK, macrophages, neutrophils, memory T cells, gamma delta, Treg, eosinophils and mast cells) following Bindea *et al*[28] for downstream comparisons, as previously performed.[7]

Single-cell RNA sequencing analysis

Two public NB scRNA-seq datasets (GSE147766 and GSE218003) were analyzed. The first includes 10 untreated patients with NB (10X Genomics), the second 19 patients (pre-chemotherapy and post-chemotherapy, Illumina NextSeq). Only samples containing B cells were retained (n=17). Datasets were initially aligned using Conos 1.2.1 (k=15, kself=5, principal component analysis (PCA) rotation space, angular distance).[29] Uniform Manifold Approximation and Projection (UMAP) visualization revealed continuous bridges connecting major populations.[30] For subtype analysis of myeloid, T, NK, or B cells, we extracted respective cells, removed low-quality samples (<50 cells), and realigned with Conos default parameters. Refined clusters were identified using Leiden clustering in Conos for higher resolution. Additional clustering results (walktrap and multilevel) are available at https://github.com/shenglinmei/NB.imzmune.atlas. To prevent overclustering, cell type/state-specific genes were evaluated. Final annotations were based on literature and cluster-specific markers. Differentially expressed genes were identified using Conos' getDifferentialGenes function. Immunotherapy response (anti-GD2, HR2 protocol) was evaluated in 13 cases; 4 were excluded due to protocol deviation or early mortality. Differential gene expression was assessed with FindMarkers between pre/post chemotherapy (n=7/10) and progression/no event groups (n=5/8).

RNA sequencing and validation

A publicly available (GSE62564) independent cohort of 498 patients with NB transcriptionally profiled by RNA-seq from the Sequencing Quality Control (SEQC) project (SEQC-NB) was employed for validation of NanoString data. Gene expression data, previously preprocessed[7 31] and stored on Gene Expression Omnibus (GEO) in the online supplemental file GSE49711_SEQC_NB_MAV_G_log2.20121127.txt.gz, were downloaded from GEO, together with patients' phenotypes, and used for downstream analyses. Additional validation was performed on The Cancer Genome Atlas (TCGA) cohorts accessed via UCSC Xena.

Statistical analysis

False discovery rate (FDR) was controlled at ≤5% using Benjamini-Hochberg correction. Hierarchical clustering used Euclidean distance and Ward linkage on log2-transformed data, visualized as scaled heatmaps. Kruskal-Wallis and Dunn's post hoc tests were used for group comparisons. Gene correlations were assessed via robust linear models, with R^2 and F-statistics reported. Overall survival (OS) and event-free survival (EFS) curves were generated using Kaplan-Meier and compared by log-rank test. Cox models estimated HRs, if the proportionality hypothesis is not met, average HRs were estimated by a weighted Cox regression model. Prognostic improvement by the B-cell gene (BCG) signature-NB was tested using logistic regression models with or without the signature. Predictive performance (Matthews Correlation Coefficient (MCC), sensitivity, specificity) was evaluated with fivefold cross-validation (10 iterations), with class downsampling. Random label permutation served as a negative control. All analyses were conducted in R using CRAN/Bioconductor libraries.

RESULTS

Tumor-infiltrating B cells predict clinical outcome in human neuroblastoma

To explore the immune cell landscape of NB, we reanalyzed scRNA-seq data from 17 patients with NB (GSE147766),[30] focusing on primary treatment-naïve tumors. Using the CONOS algorithm[29] and canonical markers,[30] we identified 10 immune cell clusters, including T, B, NK and myeloid cells (figure 1A). Among 15,432 immune cells, T cells were the most abundant (n=8,933), followed by myeloid cells (n=2,426), B cells (n=2,173), NK cells (n=1,494), type 3 innate lymphoid cells (ILC3, n=261) and plasma cells (n=145). T cells included T helper ($CD4^+$, n=4878), T cyto ($CD8^+$, n=3308) and Tregs (n=747).

Given the abundance of B cells (figure 1A) and their established prognostic role in adult cancers,[9] we investigated their significance in NB and their relationship with T-cell and DC lineages previously analyzed in the same cohort.[6–8] We found that B cells were enriched in localized (L1 and L2) compared with metastatic (M) NB (figure 1B).

To evaluate their clinical relevance in a larger cohort of NB, we analyzed *MS4A1* (CD20) expression in 498 patients with NB from the SEQC-NB (GSE62564). High *MS4A1* expression correlated with better survival (log-rank p value: 2×10^{-3}) and non-amplified MYCN status (Kruskal-Wallis rank-sum p value: 1.28×10^{-7}) (figure 1C,D). These findings were validated by IHC for CD20 on an independent cohort of 87 treatment-naïve NB cases (online supplemental table S1), previously characterized for tumor-infiltrating T, DC and NK-cell lineages, and expression of human leukocyte antigen (HLA) class I and the immune checkpoint molecules (PD-1, lymphocyte-activation gene 3 (LAG3), PD-L1).[6–8] $CD20^+$ B cells appeared as single cells or forming an organized aggregate (figure 1E), and consistent with transcriptomic data, high $CD20^+$ cell density was associated with improved OS and EFS (log-rank p values: 6.7×10^{-4} and 3.76×10^{-2}, respectively) (figure 1F,G) and more frequent in localized (L1, L2) and MYCN non-amplified NBs (log-rank p values: 6.3×10^{-6}, 2×10^{-2}, 8×10^{-3}, respectively) (figure 1H,I).

To define a transcriptional B-cell infiltration signature, we analyzed NanoString data from 36 patients with NB[7] (online supplemental table S4). Among 730 immune genes, 33 were upregulated with high *MS4A1* (fold change (FC)>2, and Q or p<0.05), 28 of which predicted better outcome (HR<1, FDR<0.05) (figure 1J, online supplemental data 1). The Primary Cell Atlas database from BioGPS revealed that 10 out of the 28 genes were primarily expressed by B, T and/or DCs (figure 1K and online supplemental figure S1) and formed a BCG signature, able to predict survival in the SEQC-NB cohort (figure 1L).

We then tested whether the BCG signature added prognostic power beyond classical predictors such as INSS stage, MYCN status, age, and T-cell infiltration. Logistic regression models showed improved performance when BCG was included (MCC: 0.50 → 0.56; sensitivity: 0.69 → 0.75; specificity: 0.79 → 0.81) (online supplemental figure S2A and online supplemental data 2). Finally, the BCG signature was validated across multiple adult tumors, demonstrating its broader clinical relevance (https://www.cancer.gov/tcga, online supplemental figure S2B,C). High expression of the BCG signature was associated with improved OS in various cancer types, including head and neck squamous cell carcinoma (HNSC), lung adenocarcinoma (LUAD), skin cutaneous melanoma (SKCM), adrenocortical carcinoma (ACC), breast carcinoma (BRCA), cervical carcinoma (CESC), colon adenocarcinomas (COAD, COADREAD), and sarcoma (SARC). These findings highlight the potential clinical significance of the BCG signature across a wide range of cancers.

Tumor-infiltrating B cells correlate with increased T-cell and DC infiltration and improved survival in human neuroblastoma

Beyond their role in humoral immunity, B cells contribute to antitumor responses.[9] Consistently, in the SEQC-NB cohort, high *MS4A1* expression correlated with transcripts linked to T-cell trafficking and cytotoxicity (eg, *CCL5, CXCL9, CXCL10, GZMA, GZMB, GZMK, ICOS* and *PRF1* online supplemental figure S3A). Similarly, the BCG signature mirrored *MS4A1* expression patterns (figure 2A). scRNA-seq revealed that $CD3^+$ T cells from $MS4A1^{high}$ patients (high B-cell levels) overexpressed genes involved in interferon signaling, adaptive and innate immunity, cytokine signaling in immune system, and immunoregulatory interactions between lymphoid and non-lymphoid cells (figure 2B,C). Using validated immune gene signatures,[28] we found a significant correlation between *MS4A1* and Bindea's BCG signature in both NanoString-NB and SEQC-NB cohorts (online supplemental figure S3B). Similar results were obtained with our BCG signature (online supplemental figure S3B). Interestingly, we found that NB samples with high levels of *MS4A1* or *CD3E* (median split) were enriched in Bindea's T-cell gene (TCG) and BCG signatures, respectively, in both NanoString-NB and SEQC-NB cohorts (figure 2D), and that transcript levels of *MS4A1* and *CD3E* were strongly correlated (figure 2E). Of note, high B-cell levels were significantly associated with better clinical outcome independently of T-cell abundance (log-rank p values: 1.5×10^{-17}) (figure 2F). These results were confirmed at the protein level by IHC staining for CD20 and CD3, both in terms of correlation and survival analysis (log-rank p values: 8.6×10^{-4} and 3.9×10^{-2} for OS and EFS, respectively) (figure 2G–I and online supplemental figure S3C). Similar data were observed for $CD4^+$ and $CD8^+$ T-cell subsets (online supplemental figures S4 and S5).

Given the mutual activation between B cells and DCs,[32 33] we explored their interaction in NB. High *MS4A1* and BCG expression correlated with markers of DC activation and maturation (CD40, CD83 and CD86) in SEQC-NB (online supplemental figure S6A). DCs

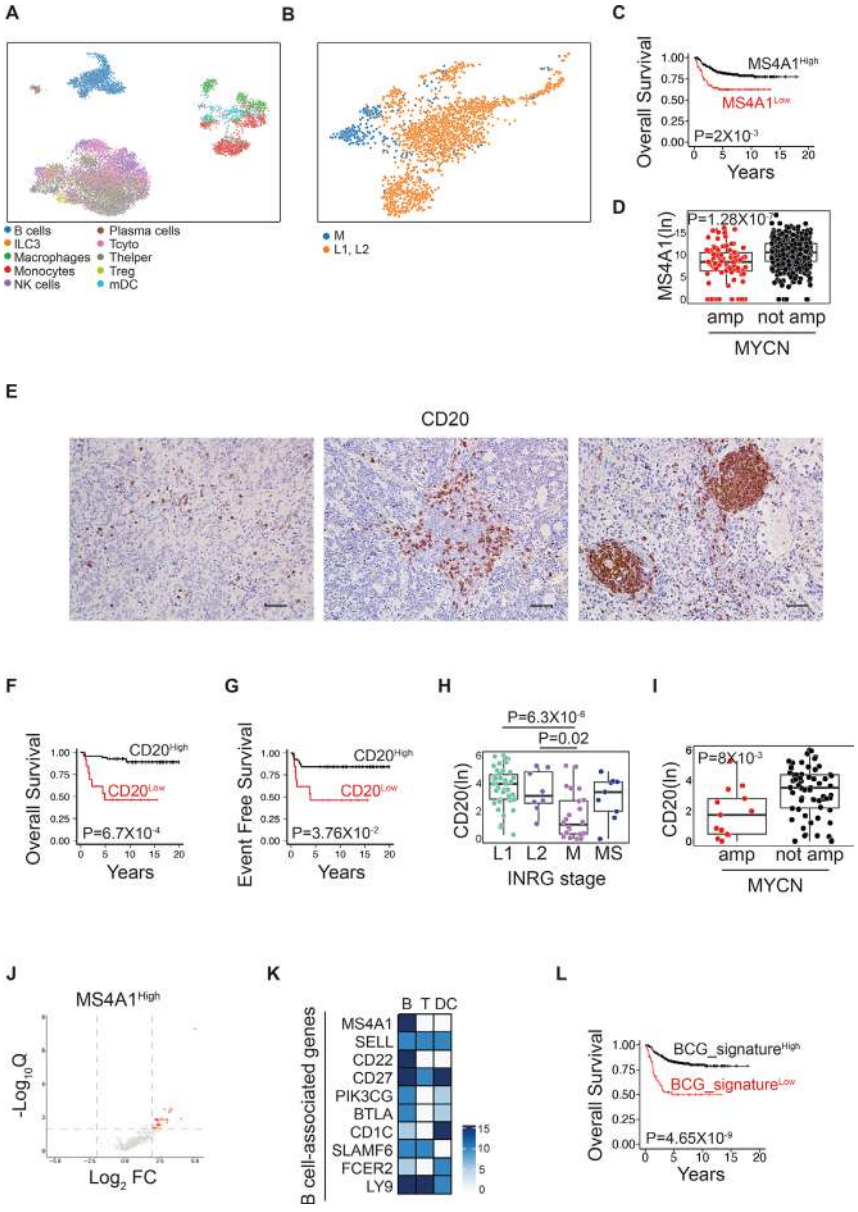

Figure 1 Tumor-infiltrating B cells are associated with favorable prognosis in patients with neuroblastoma. (A) UMAP showing the immune landscape of primary, treatment-naïve NB samples (GSE147766), comprising 15,432 single cells. Each cell is color-coded based on the annotated cell type. (B) UMAP as in (A), here highlighting the distribution of $CD20^+$ B cells in patients with localized (L1, L2) versus metastatic (M) NB. (C) Kaplan-Meier survival curves showing OS of patients with NB (SEQC-NB, n=498) stratified by *MS4A1* (CD20) gene expression. Log-rank test with Miller and Siegmund p value correction was used. (D) Box plots of *MS4A1* expression in patients with SEQC-NB according to MYCN amplification status. The boxes show the 25^{th} to 75^{th} percentile; the horizontal lines inside the box represent the median; the upper whisker extends to the largest data point, no more than 1.5 times the IQR from the box; the lower whisker extends to the smallest data point at most 1.5 times the IQR from the box; the dots are individual samples. Data were analyzed by Kruskal-Wallis rank-sum test (two-sided). (E) Representative IHC images showing $CD20^+$ B cells in primary NB lesions. CD20-expressing cells are either sparsely distributed within tumor nests (left) or clustered within irregular (middle) or regular (right) aggregates. Brown, CD20-expressing cells. Blue: hematoxylin nuclear counterstain. Original magnifications, ×20. Scale bars, 30 µm. (F–G) Kaplan-Meier curves of OS (F) and EFS (G) of patients with NB (n=87) according to the density of $CD20^+$ cells. Log-rank test with Miller and Siegmund p value correction was used. (H–I) Box plots showing $CD20^+$ cell density in patients with NB according to INRG stages (H) and MYCN amplification status (I). Dunn's multiple comparisons post hoc tests (two sides) with Benjamini-Hochberg p value adjustment and Kruskal-Wallis rank-sum test (two-sided) were employed in h and i, respectively. (J) Volcano plot showing differentially expressed immune genes associated with $MS4A1^{high}$ expression. Genes with FC>2 and Q value<0.05 are shown in red. (K) Heatmap of selected immune genes expressed by B cells and/or T cells and DCs with FC>2 and HR<1. (L) Kaplan-Meier survival curves of patients with SEQC-NB (n=498) based on the BCG signature. Log-rank test with Miller and Siegmund p value correction was used. BCG, B-cell gene; DC, dendritic cell; EFS, event-free survival; FC, fold change; IHC, immunohistochemistry; OS, overall survival; NB, neuroblastoma; SEQC, sequency quality control; UMAP, uniform manifold approximation and projection.

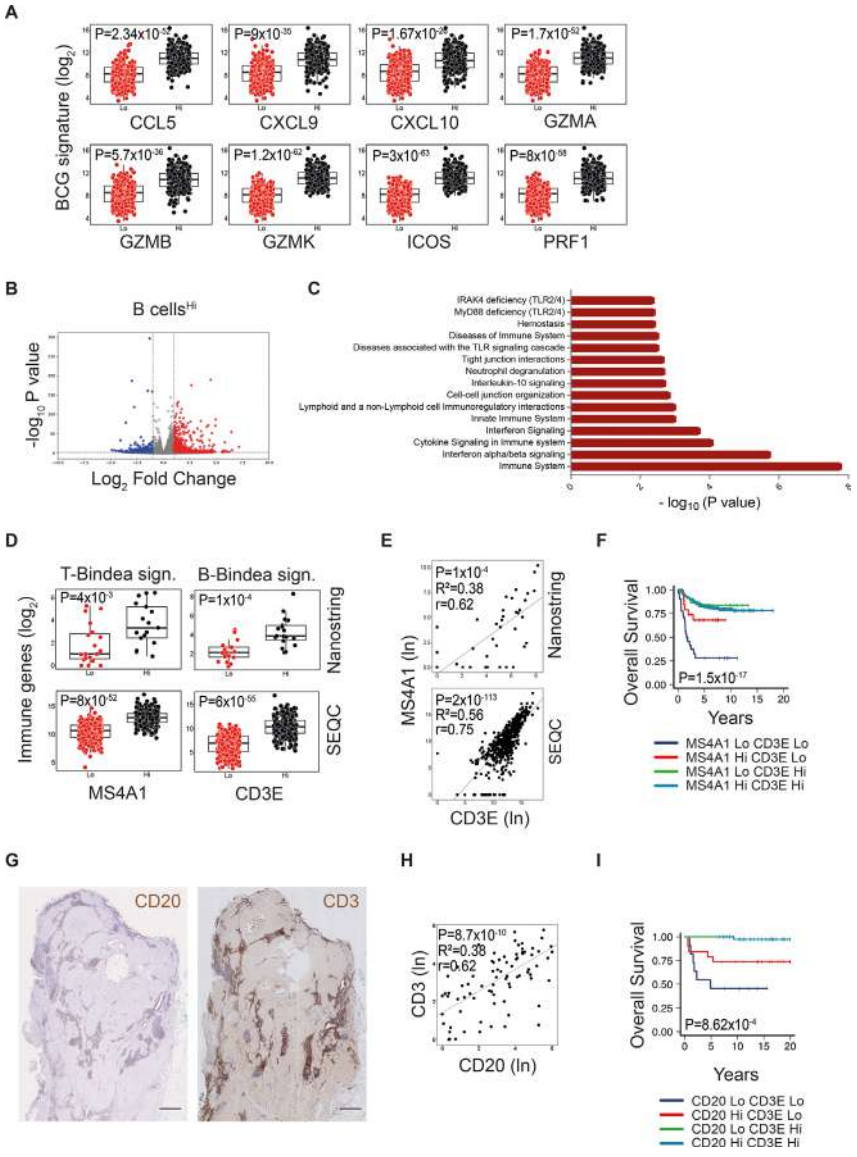

Figure 2 Intratumoral B cells correlate with increased T-cell infiltration and improved survival in patients with neuroblastoma. (A) Box plots showing expression levels of key genes involved in immune cell recruitment (CCL5, CXCL9 and CXCL10) and cytotoxic activation (GZMA, GZMB, GZMK, ICOS and PRF1), in patients with NB with high and low BCG signature in the SEQC-NB (n=498) cohort. The boxes show the 25th to 75th percentile; the horizontal lines inside the box represent the median; the whiskers extend to the most extreme data point, which is no more than 1.5 times the IQR from the box; and the dots are individual samples. P values are indicated. (B) Volcano plot showing differential gene expression in CD3$^+$ T cells (scRNA-seq, GSE147766) from patients with high B-cell levels (*MS4A1*^{high}). Genes significantly upregulated (FC>2, p value<0.05) are in red, downregulated (FC<–2, p value<0.05) are in blue. (C) Gene Ontology term enrichment analysis (via DAVID, https://david.ncifcrf.gov/) of upregulated genes in CD3$^+$ T cells from *MS4A1*^{high} patients (p value<0.05). Top 15 significantly enriched pathways are shown. (D) Box plots showing Bindea's TCG (left) and BCG (right) signatures[28] in patients with NB stratified by high/low *MS4A1* and *CD3E* expression (median split) in NanoString-NB (n=36) and SEQC-NB (n=498) cohorts. The boxes show the 25th to 75th percentile; the horizontal lines inside the box represent the median; the upper whisker extends to the largest data point, no more than 1.5 times the IQR from the box; the lower whisker extends to the smallest data point at most 1.5 times the IQR from the box; the dots are individual samples. Data were analyzed by Kruskal-Wallis rank-sum test (two-sided). (E) Correlation plots showing a positive association between *MS4A1* and *CD3E* expression in both NanoString-NB (n=36) and SEQC-NB (n=498) cohorts analyzed by robust F-test (two-sided). (F) Kaplan-Meier curves showing OS of patients with NB (n=498) according to *MS4A1* and *CD3E* expression levels. Log-rank test with Miller and Siegmund p value correction was used. (G) Representative IHC images of CD20 and CD3 staining on serial sections of NB tumors. Brown, CD20-expressing and CD3-expressing cells. Nuclei were counterstained with hematoxylin (blue). Tissue regions include tumor nests, surrounding septa, with organized aggregates. Original magnifications, ×2. Scale bars, 30 µm. (H) Scatter plot showing a positive correlation between CD20$^+$ and CD3$^+$ cell densities in patients with NB (n=87), analyzed by robust F-test (two-sided). (I) Kaplan-Meier curves showing that high density of both CD20$^+$ and CD3$^+$ cells is associated with improved OS in patients with NB (n=87). Log-rank test with Miller and Siegmund p value correction was used. BCG, B-cell gene; FC, fold change; IHC, immunohistochemistry; NB, neuroblastoma; OS, overall survival; scRNA-seq, single-cell RNA-sequencing; SEQC, sequency quality control; TCG, T-cell gene.

from *MS4A1*^{high} tumors overexpressed genes in the B-cell receptor signaling pathway (online supplemental figure S6B,C). Interestingly, tumors enriched in THBD gene expression, encoding the CD141 marker of intratumoral DCs, exhibited high levels of BCG signatures (both ours and Bindea's), in both the NanoString-NB and SEQC-NB cohorts (online supplemental figure S6D). Similarly, tumors with *MS4A1*^{high} exhibited increased expression of DCG gene (DCG) signature[7] (online supplemental figure S6D).

As for T cells, *MS4A1* and THBD transcript levels were strongly correlated in both NanoString-NB and SEQC-NB cohorts (online supplemental figure S6E), and high B-cell infiltration predicted better survival in DC-enriched NB (log-rank p value: 3.46×10^{-4}) (online supplemental figure S6F). These data were confirmed at the protein levels by IHC staining for CD20 and CD141 on serial tissues sections of NB in terms of correlation analysis (online supplemental figure S6G,H). Notably, high CD20 levels were prognostic regardless of DC abundance (log-rank p value: 1.6×10^{-3}) (online supplemental figure S6I).

Taken together, these data indicate that B cells, T cells and DCs form a cooperative immune network in NB, associated with enhanced antitumor responses and improved patient outcome.

Tertiary lymphoid structures are associated with a favorable prognosis in neuroblastoma

In our study, B cells were organized in TLSs in 68% (59 of 87) of NB samples, with 15% of these (9 of 59) being metastatic. We explored how TLS localization, morphology, cell composition, spatial distribution, and function vary across NB stages and their prognostic significance.

TLS density analysis showed that 82% of deceased patients (red dots) lack TLSs (online supplemental figure S7A). While survival analysis stratified by TLS presence revealed no significant effect on EFS (log-rank p value: 5.7×10^{-2}, online supplemental figure S7B), TLS distribution significantly differed by INRG stage and MYCN amplification, with higher densities in localized and MYCN non-amplified NBs (figure 3A,B).

TLSs were observed either within the tumor nests or at the tumor periphery,[9 15] herein referred to as intra-nest and peri-nest, respectively (figure 3C and online supplemental figure S7C). Intra-nest TLSs were more common in stages L1 and L2 NBs, whereas peri-nest TLSs predominated in stage M NBs (figure 3D).

Morphologically, TLSs ranged from a preliminary mixture of T and B cell clusters to germinal center (GC)-like structures (figure 3E). GC-like TLSs were significantly more abundant in localized stages and associated with better EFS (log-rank p value: 2.4×10^{-2}) (figure 3F,G). Interestingly, GC-like TLSs exhibit greater enrichment of B cells, CD4$^+$ and CD8$^+$ T cells, and DCs compared with non-GC-like TLSs (figure 3H and online supplemental figure S7D). scRNA-seq and NanoString analyses further revealed increased expression of two chemokines involved in TLS formation, that is, lymphotoxin B (LTB) and CXCL13,[34 35] in NBs with better prognosis (figure 3I,L).

These findings highlight the important role of TLS characteristics, such as localization, morphology, and cellular composition, in shaping the TIME and influencing NB prognosis.

Mapping TLSs in neuroblastoma by spatial proteomics

To analyze the composition, spatial organization, and functional status of B cells and other immune cells within TLSs in localized and metastatic NBs, we performed spatial proteomic using IMC. We designed a multiplexed panel of 29 antibodies to profile tumor and immune cell subtypes at subcellular resolution (online supplemental figure S8 and online supplemental table S3). From 10 NB specimens containing TLS (both localized and metastatic NBs, online supplemental table S5), we acquired 100 high-dimensional histopathology images. Using a deep-learning algorithm,[36] we were able to perform cell segmentation, identifying 812,491 single cells.

Immune cells were identified using the pan-immune marker CD45 and clustered based on protein expression, resulting in the classification of 15 immune and 5 non-immune major cell phenotypes (online supplemental figure S9). Among the non-immune cells, populations expressing CD71, TIM3, HLA-DR and IL7RA, or CD71 plus IL7RA were detected (online supplemental figure S9C). Previous studies have reported expression of CD71, TIM3 and HLA-DR on NB cells.[37–39] Notably, HLA-DR$^+$ non-immune cells were significantly less frequent in stage M NB, whereas clusters expressing CD71, IL7RA and CD71/IL7RA exhibited an opposite trend (online supplemental figure S10A and online supplemental table S6). Within immune cells, distinct B-cell subsets were identified (CD79$^+$CD3$^-$), including memory (CD79$^+$CD3$^-$CD20$^+$CD27$^+$), naïve (CD79$^+$CD3$^-$CD20$^+$CD27$^-$) and plasma cells (CD79$^+$CD3$^-$CD20$^-$CD27$^-$) (online supplemental figure S9). Among naïve B cells, two clusters were distinguished based on IL7RA expression (online supplemental figure S9). T-cell subsets (CD79$^-$CD68$^-$CD14$^-$HLA-DR$^-$CD3$^+$) were classified into cytotoxic (CD8$^+$), helper (CD4$^+$), and Treg cells (CD4$^+$FOXP3$^+$) (online supplemental figure S9). An example of segmentation for B-cell and T-cell populations is shown in online supplemental figure S10B. Additionally, two immune cell populations co-expressing high levels of HLA-DR and either CD4 or CD8, but lacking CD3, were identified (online supplemental figures S9 and S10C). Macrophages (M1-like: CD68$^+$CD163$^-$; M2-like: CD68$^+$CD163$^+$), monocytes (CD68$^-$CD14$^+$) and DCs (CD68$^-$CD14$^-$HLA-DR$^+$CD11c$^+$CD11b$^-$) were also reported (online supplemental figures S9 and S10C).

TLSs exhibit a mature state with dense accumulations of diverse B- and T-cell subtypes in localized NBs

UMAP analysis revealed that the 15 immune cell clusters were unevenly distributed across stages, being generally less abundant in metastatic NBs (figure 4A, online

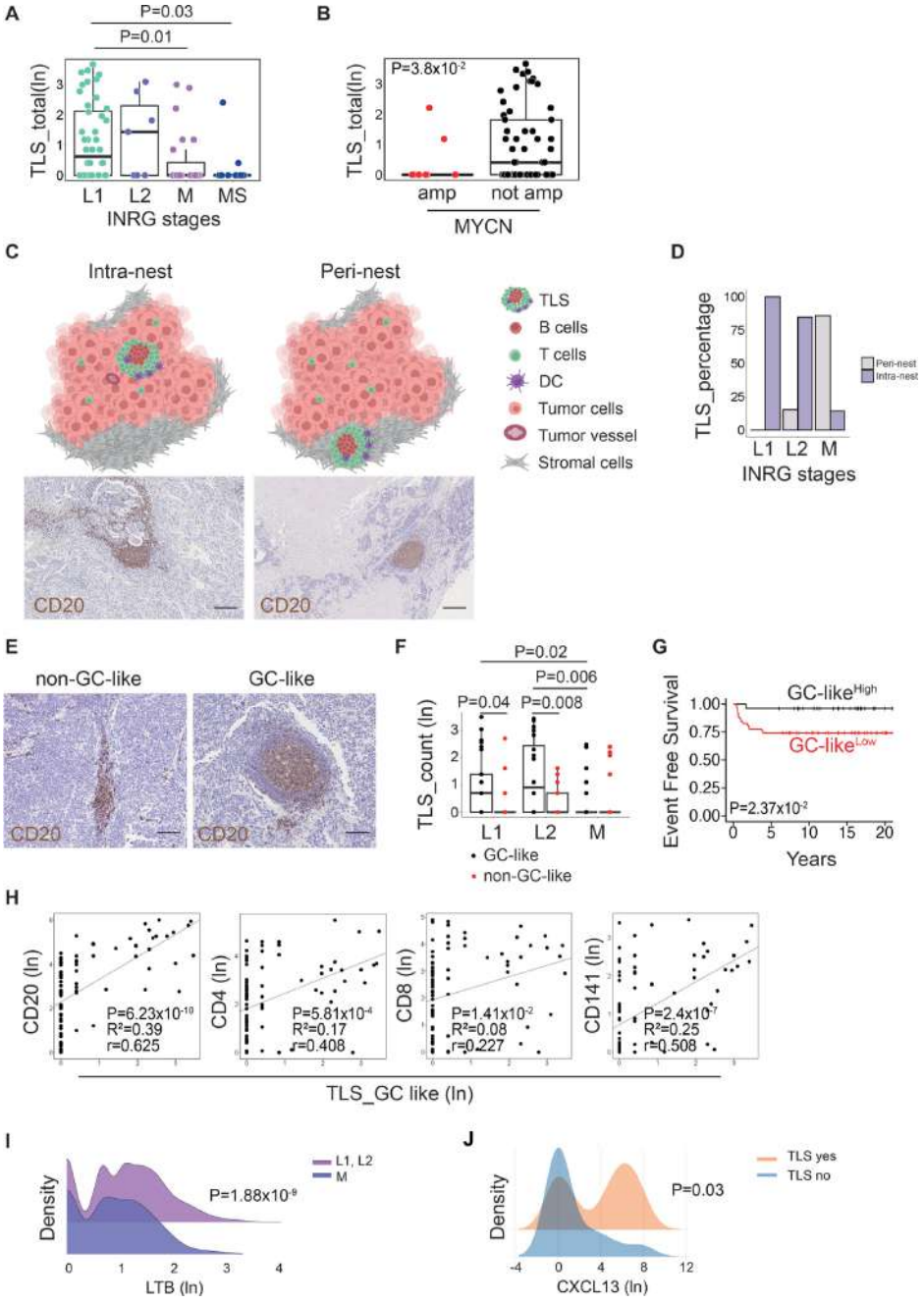

Figure 3 Clinical relevance of tumor-infiltrating TLSs in neuroblastoma. (A–B) Box plots showing the number of TLSs stratified by INRG stages (A) and MYCN amplification status (B) in NB lesions (n=87). Dunn's multiple comparisons post hoc tests (two sides) with Benjamini-Hochberg p value adjustment and Kruskal-Wallis rank-sum test (two-sided) were employed in (A) and (B), respectively. (C) Schematic illustrating spatial organization of TLSs: intra-nest TLSs, located within the tumor nest, and peri-nest TLSs, positionated in the tumor septa (top). Representative CD20 immunostaining images of both TLS types are shown (bottom). Brown, CD20-expressing cells; nuclei counterstained with hematoxylin (blue). Original magnifications, ×10. Scale bars, 30 µm. (D) Bar chart showing distribution of intra-nest versus peri-nest TLSs across different INRG stages in TLS$^+$ patients (n=42). (E) Representative CD20 staining of GC-like and non-GC-like TLSs in primary NB specimens. Brown, CD20-expressing cells, nuclei counterstained with hematoxylin (blue). Original magnifications, ×20. Scale bars, 30 µm. (F) Box plots comparing the frequency of GC-like and non-GC-like TLSs across INRG stages. Dunn's multiple comparisons post hoc tests (two sides) with Benjamini-Hochberg p value adjustment were employed. (G) Kaplan-Meier curves of EFS of patients with NB (n=87) according to GC-like TLS density. Log-rank test with Miller and Siegmund p value correction was used. (H) Scatter plots showing correlations between GC-like TLSs and densities of CD20$^+$, CD4$^+$, CD8$^+$ or CD141$^+$ immune cells in patients with NB (n=87), analyzed by robust F-test (two-sided). (I) Density plots of LTB expression in B cells from patients with localized versus metastatic NB (scRNA-seq, GSE147766) analyzed by Mann-Whitney U test. (L) Density plots of CXCL13 expression in NanoString-NB (n=36) stratified by TLS presence and evaluated using the Mann-Whitney U test. EFS, event-free survival; GC, germinal center; LTB, lymphotoxin B; NB, neuroblastoma; scRNA-seq, single-cell RNA-sequencing; TLSs, tertiary lymphoid structures.

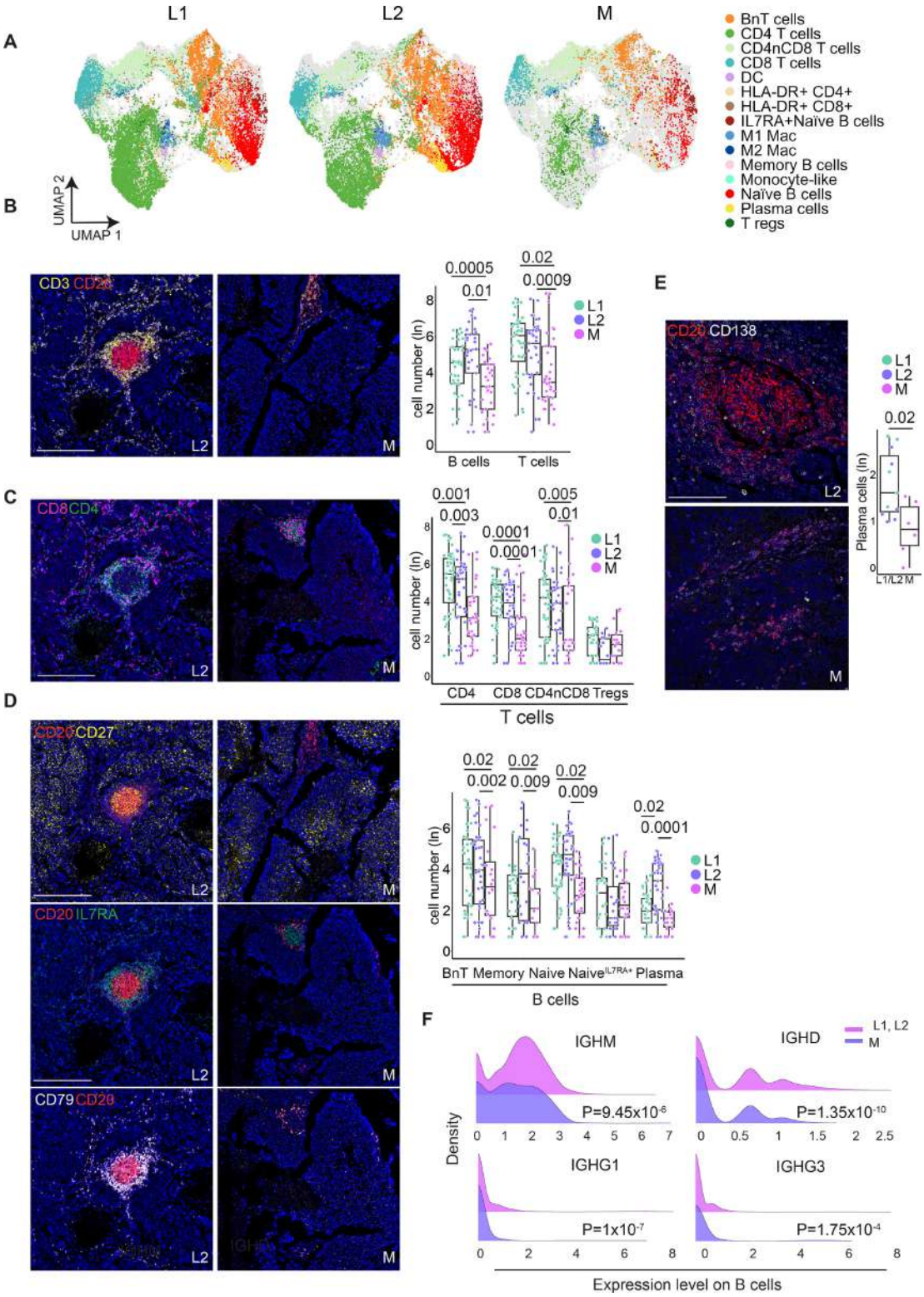

Figure 4 Distinct spatial immune composition of TLSs in localized and metastatic neuroblastoma. (A) UMAP plots of immune cells identified by IMC across NB lesions, showing 15 clusters according to INRG stages. (B–D) Representative ROIs from TLSs in localized and metastatic NB visualized by IMC, showing spatial distribution of B-cell and T-cell subsets. Scale bar=170 µm. Box plots compare immune subset frequency by INRG stage. Dots represent individual ROIs. Kruskal-Wallis test followed by Dunn's multiple comparisons was used. (E) Immunofluorescence staining of CD20 (red) and CD138 (white) in TLSs from localized and metastatic tumors. Nuclei stained with Hoechst. Magnification ×40, scale bar 30 µm. The right panel shows quantification of plasma cells (n=19). Kruskal-Wallis test was used. (F) Density plots of Ig gene expression in B cells from patients with localized and metastatic NB (scRNA-seq, GSE147766). Mann-Whitney U test was used. IMC, imaging mass cytometry; NB, neuroblastoma; ROIs, regions of interest; scRNA-seq, single-cell RNA-sequencing; TLSs, tertiary lymphoid structures; UMAP, uniform manifold approximation and projection.

supplemental figure S10D). In localized NBs, TLSs feature a core of proliferating (Ki67$^+$) B cells surrounded closely by CD4$^+$ T cells, and CD8$^+$ T cells expressing PD-1, resembling GC (GC-like TLS) (figure 4B,C, online supplemental figure S10E). In contrast, metastatic NBs display disorganized TLSs (non-GC-like TLS) with scattered T and B cells or T-cell aggregates surrounded by few B cells (figure 4B,C, online supplemental figure S10F), positioned towards the periphery of the tumor nest (peri-nest). The B cells that populate the center of TLSs in localized NBs are mostly memory and naïve, whereas plasma cells reside outside these structures (figure 4D). The localization of plasma cells was confirmed by IF (CD20$^-$CD138$^+$)[40] in a larger cohort (n=19) (figure 4E, online supplemental table S7). Quantitative analysis revealed significantly fewer memory B cells, IL7RA$^-$ naïve B cells, and plasma cells in TLSs of metastatic NBs (figure 4D,E). In line, scRNA-seq showed an enrichment of immunoglobulin (Ig) transcripts (*IGHM*, *IGHD*, *IGHG1* and *IGHG3*) in B cells from localized NBs (figure 4F, online supplemental figure S11A). Regarding T-cell subsets, all but Treg were significantly less abundant in metastatic NBs (figure 4C). DCs and HLA-DR$^+$CD4$^+$ and HLA-DR$^+$CD8$^+$ (CD3$^-$) populations localized mainly in the TLS, regardless of maturity, and were more abundant in stages L1 and L2 (online supplemental figure S11B,C). Other myeloid cells, including macrophages and monocytes, were absent in TLSs and less represented in stage M NBs (online supplemental figure S11D).

Taken together, these results indicate that TLSs in localized NBs are more mature and display greater diversity in B-cell and T-cell subtypes compared with those in metastatic NB, further supporting that the organization and diversity of the TIME is essential for a more effective antitumor immune response.

TLSs in metastatic neuroblastomas exhibit dysfunctional B-cell and T-cell subpopulations

The functional properties of the B-cell and T-cell subtypes infiltrating TLSs were assessed by the expression of differentiation and exhaustion markers (figure 5A–D, online supplemental figure S12A–E). B cells of metastatic NB tissues exhibited a phenotype characteristic of dysfunctional populations (figure 5A,B, online supplemental figure S12A–C). Memory and naïve B cells (both IL7RA$^+$ and IL7RA$^-$) showed reduced HLA-DR levels, suggesting diminished antigen-presenting capacity[14] (figure 5A, online supplemental figure S12C). Additionally, memory B cells expressed low CCR6 and PD-1, which are essential for effective antigen responses[41 42] (figure 5B, online supplemental figure S12B,C). T cells in metastatic TLSs also showed dysfunction, with CD4$^+$ and CD8$^+$ T-cell subsets expressing high TIM3 and IL7RA, but reduced granzyme B (figure 5C and online supplemental figure S12D,E). Inducible T-cell costimulator (ICOS) and PD-1 were downregulated in CD8$^+$ and CD4$^+$ T cells, respectively (figure 5C and online supplemental figure S12E). This phenotype was accompanied by increased proliferating Treg cells or expressing T-box transcription factor (Tbet) (figure 5D), known to suppress cytotoxic T-cell activity.[43] Non-immune cells also exhibited increased proliferation in metastatic NB (online supplemental figure S12F).

Next, to gain insight into the tumor architecture, we compared the strength of spatial interactions across L1, L2 and M NB samples (figure 5E, online supplemental data 3). In metastatic NBs, TIM3$^+$ non-immune cells interacted more strongly with CD8$^+$ T cells, but less with M1 macrophages compared with localized tumors (figure 5E, online supplemental data 3). HLA-DR$^+$ non-immune cells had reduced interactions with CD4$^+$ T cells and naïve B cells (figure 5E, online supplemental data 3). Immune cell interactions were generally weaker (figure 5E), with IL7RA$^-$ naïve B cells showing decreased interaction with memory B cells, CD4$^+$ and CD8$^+$ T cells and M1 macrophages. Similarly, plasma cells and IL7RA$^+$ naïve B cells had reduced interaction with CD4$^+$ T cells and memory B cells, respectively (figure 5E, online supplemental data 3). CD4$^+$ and CD8$^+$ T cells interacted less with each other and with M1 macrophages, whereas DCs engaged less with CD4$^+$ T cells, HLA-DR$^+$ CD4$^+$ cells and M1 macrophages.

This multitude of immunoregulatory interactions underscores TLSs as hubs of immune coordination, with CD4$^+$ T cells and IL7RA$^-$ naïve B cells as central interacting players in the TIME of localized NB, a network disrupted in metastatic disease.

TLS gene signature and immunoglobulin expression predict prognosis and treatment response in neuroblastoma

To assess the prognostic significance of TLSs in NB, we developed a TLS gene signature (TLSG) based on NanoString profiling of patients with NB with TLS presence confirmed by IHC. Genes were selected using the following criteria: FC>2 or <−2 and p value<0.05, strong prognostic value (HR<1 or >1), and expression by TLS components, that is, B cells, T cells and DCs (online supplemental data 4).

Out of 730 immune-related genes, 11 were upregulated in TLS-positive samples, 9 of which were correlated with favorable prognosis. Six of these were expressed in B, T and/or DCs (figure 6A,B, online supplemental figure S13 and data 4). Unsupervised clustering based on these six TLS genes revealed a distinct patient group with improved survival in the SEQC-NB dataset (figure 6C, online supplemental figure S14A). The derived TLSG signature was validated across adult cancers (online supplemental figure S14B–D). High expression of the TLSG signature was associated with improved OS in several cancer types, including BRCA, CESC, COAD, COAD-READ, HNSC, LUAD, SARC, SKCM and uterine carcinosarcoma (https://www.cancer.gov/tcga). Notably, this TLSG signature outperformed a previously published TLSG signature[44] (online supplemental figure S14D).

To explore the predictive value of the TLSG signature for therapy response, we analyzed scRNA-seq data from 13 patients with metastatic NB treated with the HR2 protocol, including anti-GD2 immunotherapy (online

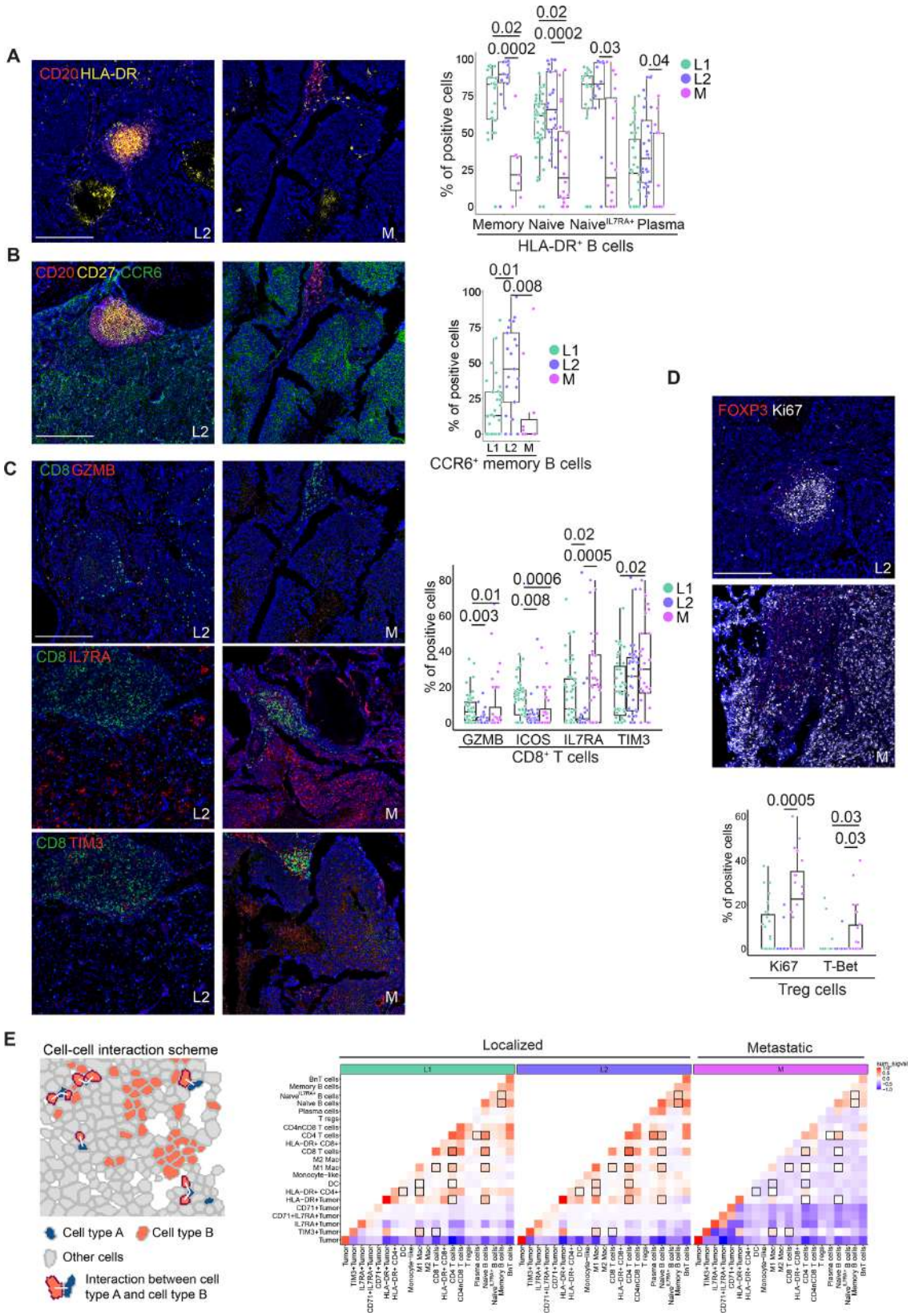

Figure 5 TLSs are associated with antitumor adaptive immunity in neuroblastoma. (A–D) IMC-based analysis of TLSs in localized and metastatic NB lesions. Antibody overlays reveal B-cell and T-cell subtypes key functional markers. Scale bar=170 µm. Box plots compare marker-positive cell proportions by INRG stage. Dots represent single ROIs. Kruskal-Wallis test followed by Dunn's multiple comparisons was used. (E) Schematic representation of homotypic and heterotypic cell–cell interaction metrics (left) and heatmap of Pairwise Interaction Avoidance Scores (red, strong interaction; blue, strong avoidance) illustrating interaction/avoidance patterns of immune populations across NB stages. IMC, imaging mass cytometry; NB, neuroblastoma; ROIs, regions of interest; TLSs, tertiary lymphoid structures.

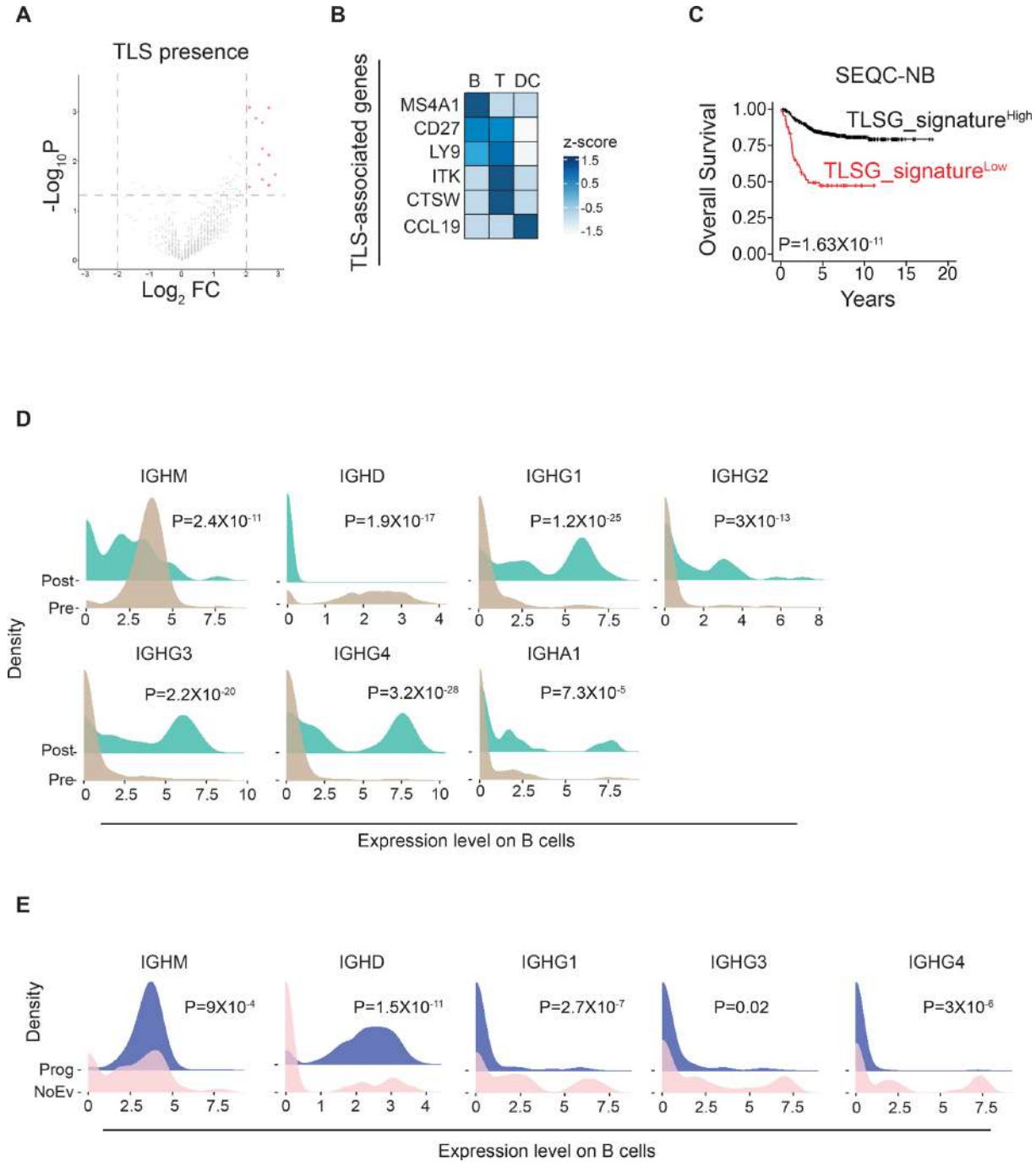

Figure 6 TLS gene signature and immunoglobulin expression predict patient outcome and treatment response. (A) Volcano plot showing differentially expressed immune genes in TLS$^+$ versus TLS$^-$ NB samples. Upregulated genes (FC>2, p<0.05) are highlighted in red. (B) Heatmap of B-, T- and DC-related genes upregulated in TLS$^+$ tumors and associated with favorable prognosis (FC>2, HR<1). (C) Kaplan-Meier curves showing OS of patients with NB (n=498), stratified by the TLSG signature. Log-rank test with Miller and Siegmund p value correction was used. (D–E) Density plots showing Ig genes in B cells and plasma cells from (D) untreated (pre, n=7) versus treated (post, n=10) metastatic NB samples, and (E) responding (No Ev, n=8) versus non-responding (Prog, n=5) from scRNA-seq dataset GSE218003. Differential expression analysis was conducted using FindAllMarkers with Bonferroni p value correction. DC, dendritic cell; FC, fold change; NB, neuroblastoma; OS, overall survival; scRNA-seq, single-cell RNA-sequencing; TLS, tertiary lymphoid structures; TLSG, TLS gene signature.

supplemental table S1 in[45]). Five patients progressed, while eight showed no disease events. The expression of these genes did not differ significantly between patients that had no event during immunotherapy and those that had progression of disease during or shortly after immunotherapy (online supplemental figure S15A). These genes were either low or undetectable in both groups (online supplemental figure S15B), suggesting the TLSG signature has prognostic but not predictive value for immunotherapy response.

Given the reported link between TLSs and Ig-producing plasma cells in other tumors,[46 47] we examined Ig gene expression after induction chemotherapy. scRNA-seq data from 7 untreated and 10 treated patients with NB showed a shift from B cells to plasma cells post-treatment (online supplemental figure S15C,D). Chemotherapy-treated patients had higher levels of *IGHG1-4* and *IGHA1,* and lower *IGHM* and *IGHD*, consistent with class switching from naïve/memory B cells to antibody-producing plasma cells (figure 6D and online supplemental figure S15E). This pattern likely reflects the fact that *IGHM* and *IGHD* are primarily expressed by naïve B cells and, to some extent, memory B cells, both of which are proliferating and chemotherapy-sensitive. In contrast, *IGHG1-4* and *IGHA1* are expressed by plasma cells, which are differentiated and chemotherapy-resistant. Interestingly, we observed that the expression of *IGHM* and *IGHD* genes was higher in patients with progressive disease during or shortly after immunotherapy with anti-GD2 compared with those without an event during immunotherapy, while *IGHG1, IGHG3* and *IGHG4* were lower in patients with progressive disease (figure 6E, and online supplemental figure S15F).

Collectively, these findings highlight that the TLSG signature serves as a strong prognostic marker in NB, while the expression levels of Ig genes may provide additional insights into response to anti-GD2 immunotherapy.

DISCUSSION

In this study, we provide evidence for the prognostic relevance, spatial organization, and functional role of tumor-infiltrating B cells and TLSs in NB, using both a well-characterized patient cohort and publicly available bulk and scRNA-seq datasets.[6–8 30 45] Our transcriptomic and proteomic analyses demonstrate that tumors enriched in B cells are associated with improved patient outcomes, particularly when B cells co-occur with $CD4^+$ and $CD8^+$ T cells as well as DCs, underscoring the importance of a coordinated immune response.

We observed that B cells can either be dispersed throughout the tumor or arranged within TLSs of variable maturity. Localized NBs were enriched in mature TLSs resembling GCs. These structures featured central clusters of naïve and memory proliferating B cells, surrounded by $CD4^+$ T cells and peripheral $CD8^+$ T cells, both expressing PD-1. This spatial organization suggests an active and productive TIME. In contrast, metastatic NB displayed few, predominantly immature TLSs, in which B and T cells appeared disorganized and functionally impaired.

These findings align with studies in adult cancers, where TLSs of high maturity often correlate with improved prognosis and evidence of active B-cell differentiation into antibody-secreting plasma cells.[48] In many tumors, TLSs contain highly differentiated B cells capable of producing tumor-specific antibodies and promoting effective T-cell responses.[49] Conversely, in renal cell carcinoma, TLSs are frequently less organized, lack GC-like structures, and have even been associated with poorer prognosis.[50 51] Our observations in NB therefore position this disease closer to "immunologically active" adult tumors, where the presence of mature TLSs reflects a functional immune compartment that supports antitumor activity.

The functional relevance of B-cell activation in TLSs is further supported by our findings on Ig expression. In localized NB, we detected high levels of *IGHM*, *IGHD*, and *IGHG*, consistent with the presence of naïve, memory, and functional B cells. In adult tumors, such as melanoma, IgG^+ plasma cells within TLSs have been associated with favorable responses to ICIs, likely through the production of tumor-specific antibodies and the formation of immune complexes that enhance antigen presentation by DCs.[9] By contrast, tumors with immature TLSs often display reduced class switching and limited plasma cell differentiation.[9] Thus, our data extend observations from other cancer types, supporting a model in which TLS maturity is tightly linked to the differentiation state of B cells and the functional quality of the immune response.

Beyond antibody production, B cells in NB TLSs showed robust antigen presentation, with HLA class II expression in naïve and memory B-cell subsets.[14] Memory B cells expressed CCR6 and PD-1, functional markers and of relevance for B-cell migration and plasma cell differentiation.[52] The loss of CCR6 has been shown in other systems to impair B-cell positioning and terminal differentiation,[52] further underscoring the role of TLS architecture in shaping immune responses. Consistent with these mechanisms, NB patients with high B-cell content showed enrichment of genes involved in cytotoxic T-cell recruitment, DC maturation, interferon signaling, and T-cell activation, all indicators of an active TIME.

In metastatic NB, TLS-infiltrating $CD4^+$ and $CD8^+$ T cells exhibited features of exhaustion, with high TIM3 and low granzyme B expression, similar to what has been observed in immunotherapy-resistant melanoma.[44] The TIME was further characterized by proliferating Tregs, including $Tbet^+$ subsets known to dampen type 1 helper responses.[43] We also found IL7RA expression, a marker of long-lived memory T cells, on $CD4^+$ and $CD8^+$ T cells in metastatic TLSs, suggesting residual immune potential even within a dysfunctional microenvironment. This raises the possibility that immature TLSs, while less effective than their mature counterparts, may still provide partial immune protection.

Importantly, TLSs in localized NB contained functional DCs and $PD1^+$ T cells that support B-cell activation and differentiation,[53] and correlated with the expression of lymphoid neogenesis markers such as LTB and CXCL13, previously reported as predictive of TLS presence in several cancers.[20] Localized NBs also showed $CD4^+$ and $CD8^+$ T cells expressing granzyme B, PD-1, and ICOS, which can support B-cell activation and TLS function.[54] These findings suggest that, in mature TLSs, PD-1 expression on resident T cells may reflect immune modulation rather than T-cell exhaustion.[55]

Clinically, TLS density, particularly intratumoral and GC-like TLSs, strongly correlated with favorable outcomes.[15 20] Accordingly, our BCG and TLSG gene signatures independently predicted prognosis, offering new biomarkers for NB risk stratification. Of note, patients with NB responding to anti-GD2 immunotherapy displayed increased IgG gene expression, echoing reports in adult tumors where IgG^+ plasma cells correlate with responsiveness to ICIs.[13 17 44] Plasma cells may contribute to therapy efficacy by producing tumor-specific antibodies and forming antigen-antibody complexes that are internalized by DCs, thereby amplifying T-cell responses and synergizing with immunotherapy.[56]

Overall, our study provides a comprehensive view of B-cell infiltration, TLS composition, and immune interactions in NB. By comparing our data with findings from other solid tumors, we highlight that TLS maturity and B-cell differentiation states are crucial determinants of prognosis and immune functionality. We demonstrate that the compartmentalization of lymphocytes within fully developed TLSs supports potent antitumor immunity, whereas immature TLSs are associated with disorganized and exhausted immune populations. Finally, our identification of BCG and TLSG gene signatures refines prognostic assessment in NB and underscores the clinical potential of TLS-associated and B cell-associated features as biomarkers. These insights support future strategies aimed at remodeling the TIME in metastatic NB, promoting TLS maturation, and potentially enhancing the efficacy of immunotherapies in pediatric patients.

Author affiliations
[1]Department of Pediatric Hematology and Oncology, Bambino Gesù Children's Hospital IRCCS, Rome, Italy
[2]Department of Clinical Sciences and Translational Medicine, University of Rome Tor Vergata, Rome, Italy
[3]Data Science for Health, Fondazione Bruno Kessler Research Center, Trento, Italy
[4]Princess Máxima Center for Pediatric Oncology, Utrecht, The Netherlands
[5]Division of Pediatric Oncology and Pediatric Surgery, Department of Women's and Children's Health, Karolinska Institutet, Stockholm, Sweden
[6]Department of Biomedical Sciences, Humanitas University, Pieve Emanuele (Milan), Italy
[7]Department of Life Sciences and Public Health, Catholic University of the Sacred Heart, Rome, Italy

Contributors DF coordinated the project and provided the findings. DF and OM conceived and designed experiments, developed methodologies, acquired, analyzed and interpreted the data, and wrote the paper. OM performed the experiments. MC and PG preprocessed RNA-seq datasets and IMC data, respectively, as well as performed statistical analyses and generated plots. NL, JW, and FJB preprocessed the scRNA-seq datasets, performed statistical analyses, and generated plots. GJ provided critical support for statistical analyses and contributed to plot generation. LLP and MV contributed to IMC experiments. CDS, VD'O, and MCB contributed to IHC and IF experiments. RA, MADI, and FL contribute to acquire and manage patients. GB, MV, RC, JJM, and FL discussed the results and provided critical comments. All authors critically revised and edited the paper. DF is the guarantor.

Funding This work was supported by grants awarded by the Associazione Italiana Ricerca sul Cancro (AIRC) IG18495 (DF) and IG24345 (DF), the Italian Ministry of Health with Ricerca Finalizzata No. PE-2011–02351866 (DF), Current Research funds (DF), the European Union's Horizon 2020 research and Innovation program under the Marie Skłodowska-Curie Actions grant agreement No 954992 (CAPSTONE-ETN) (DF). This research was also supported by one fellowship from the Fondazione Umberto Veronesi (FUV) (LLP) and a CAPSTONE-ETN H2020 Early Stage Researchers (PG).

Competing interests No, there are no competing interests.

Patient consent for publication Not applicable.

Ethics approval This study was approved by the Ethics Committee of the Ospedale Pediatrico Bambino Gesù of Rome, Italy. Reference number for ethics approval is Fruci_1337_OPBG. Written informed consent was obtained for each patient in accordance with the Declaration of Helsinki prior to the initiation of the experiments.

Provenance and peer review Not commissioned; externally peer reviewed.

Data availability statement Data are available in a public, open access repository. Data are available upon reasonable request. All data relevant to the study are included in the article or uploaded as supplementary information. The authors declare that all data supporting the findings of this study are available within the paper and its supplementary information files. The bioinformatic investigation was performed by querying gene expression cancer datasets from GEO GSE62564, GSE147766 and GSE218003 for NB (DOIs: 10.1186/s13059-015-0694-1, DOI: 10.1016/j.xcrm.2022.100657, doi: 10.1016/j.ccell.2023.12.008, respectively), and from TCGA Research Network (https://www.cancer.gov/tcga) for LUAD, HNSC and SKCM. Primary Cell Atlas database from BioGPS (http://biogps.org) was used to refine the B cell and TLS gene signatures. IMC raw data are available in the Zenodo repository.[57] Any other relevant data and code are available from the corresponding author upon reasonable request.

ORCID iD
Doriana Fruci https://orcid.org/0000-0003-3388-7296

REFERENCES

1 Melaiu O, Lucarini V, Giovannoni R, *et al*. News on immune checkpoint inhibitors as immunotherapy strategies in adult and pediatric solid tumors. *Semin Cancer Biol* 2022;79:18–43.
2 Smith MA, Seibel NL, Altekruse SF, *et al*. Outcomes for children and adolescents with cancer: challenges for the twenty-first century. *J Clin Oncol* 2010;28:2625–34.
3 Wienke J, Dierselhuis MP, Tytgat GAM, *et al*. The immune landscape of neuroblastoma: Challenges and opportunities for novel therapeutic strategies in pediatric oncology. *Eur J Cancer* 2021;144:123–50.
4 Lucarini V, Melaiu O, D'Amico S, *et al*. Combined mitoxantrone and anti-TGFβ treatment with PD-1 blockade enhances antitumor immunity by remodelling the tumor immune landscape in neuroblastoma. *J Exp Clin Cancer Res* 2022;41:326.
5 Tempora P, D'Amico S, Gragera P, *et al*. Combining ERAP1 silencing and entinostat therapy to overcome resistance to cancer immunotherapy in neuroblastoma. *J Exp Clin Cancer Res* 2024;43:292.
6 Mina M, Boldrini R, Citti A, *et al*. Tumor-infiltrating T lymphocytes improve clinical outcome of therapy-resistant neuroblastoma. *Oncoimmunology* 2015;4:e1019981.
7 Melaiu O, Chierici M, Lucarini V, *et al*. Cellular and gene signatures of tumor-infiltrating dendritic cells and natural-killer cells predict prognosis of neuroblastoma. *Nat Commun* 2020;11:5992.
8 Melaiu O, Mina M, Chierici M, *et al*. PD-L1 Is a Therapeutic Target of the Bromodomain Inhibitor JQ1 and, Combined with HLA Class I, a Promising Prognostic Biomarker in Neuroblastoma. *Clin Cancer Res* 2017;23:4462–72.
9 Fridman WH, Meylan M, Pupier G, *et al*. Tertiary lymphoid structures and B cells: An intratumoral immunity cycle. *Immunity* 2023;56:2254–69.

10 Hu X, Zhang J, Wang J, *et al*. Landscape of B cell immunity and related immune evasion in human cancers. *Nat Genet* 2019;51:560–7.
11 Biswas S, Mandal G, Payne KK, *et al*. IgA transcytosis and antigen recognition govern ovarian cancer immunity. *Nature New Biol* 2021;591:464–70.
12 Nielsen JS, Sahota RA, Milne K, *et al*. CD20+ tumor-infiltrating lymphocytes have an atypical CD27- memory phenotype and together with CD8+ T cells promote favorable prognosis in ovarian cancer. *Clin Cancer Res* 2012;18:3281–92.
13 Petitprez F, de Reyniès A, Keung EZ, *et al*. B cells are associated with survival and immunotherapy response in sarcoma. *Nature New Biol* 2020;577:556–60.
14 Laumont CM, Nelson BH. B cells in the tumor microenvironment: Multi-faceted organizers, regulators, and effectors of anti-tumor immunity. *Cancer Cell* 2023;41:466–89.
15 Schumacher TN, Thommen DS. Tertiary lymphoid structures in cancer. *Science* 2022;375:eabf9419.
16 Dieu-Nosjean MC. Tumor-Associated Tertiary Lymphoid Structures: A Cancer Biomarker and a Target for Next-generation Immunotherapy. *Adv Exp Med Biol* 2021;1329:51–68.
17 Vanhersecke L, Brunet M, Guégan J-P, *et al*. Mature tertiary lymphoid structures predict immune checkpoint inhibitor efficacy in solid tumors independently of PD-L1 expression. *Nat Cancer* 2021;2:794–802.
18 Lynch KT, Young SJ, Meneveau MO, *et al*. Heterogeneity in tertiary lymphoid structure B-cells correlates with patient survival in metastatic melanoma. *J Immunother Cancer* 2021;9:e002273.
19 Posch F, Silina K, Leibl S, *et al*. Maturation of tertiary lymphoid structures and recurrence of stage II and III colorectal cancer. *Oncoimmunology* 2018;7:e1378844.
20 Silina K, Soltermann A, Attar FM, *et al*. Germinal Centers Determine the Prognostic Relevance of Tertiary Lymphoid Structures and Are Impaired by Corticosteroids in Lung Squamous Cell Carcinoma. *Cancer Res* 2018;78:1308–20.
21 Irwin MS, Naranjo A, Zhang FF, *et al*. Revised Neuroblastoma Risk Classification System: A Report From the Children's Oncology Group. *J Clin Oncol* 2021;39:3229–41.
22 Mathew P, Valentine MB, Bowman LC, *et al*. Detection of MYCN gene amplification in neuroblastoma by fluorescence in situ hybridization: a pediatric oncology group study. *Neoplasia* 2001;3:105–9.
23 Kohler JA, Rubie H, Castel V, *et al*. Treatment of children over the age of one year with unresectable localised neuroblastoma without MYCN amplification: results of the SIOPEN study. *Eur J Cancer* 2013;49:3671–9.
24 Rubie H, De Bernardi B, Gerrard M, *et al*. Excellent outcome with reduced treatment in infants with nonmetastatic and unresectable neuroblastoma without MYCN amplification: results of the prospective INES 99.1. *J Clin Oncol* 2011;29:449–55.
25 De Bernardi B, Mosseri V, Rubie H, *et al*. Treatment of localised resectable neuroblastoma. Results of the LNESG1 study by the SIOP Europe Neuroblastoma Group. *Br J Cancer* 2008;99:1027–33.
26 De Ioris MA, Castellano A, Ilari I, *et al*. Short topotecan-based induction regimen in newly diagnosed high-risk neuroblastoma. *Eur J Cancer* 2011;47:572–8.
27 Windhager J, Zanotelli VRT, Schulz D, *et al*. An end-to-end workflow for multiplexed image processing and analysis. *Nat Protoc* 2023;18:3565–613.
28 Bindea G, Mlecnik B, Tosolini M, *et al*. Spatiotemporal dynamics of intratumoral immune cells reveal the immune landscape in human cancer. *Immunity* 2013;39:782–95.
29 Barkas N, Petukhov V, Nikolaeva D, *et al*. Joint analysis of heterogeneous single-cell RNA-seq dataset collections. *Nat Methods* 2019;16:695–8.
30 Verhoeven BM, Mei S, Olsen TK, *et al*. The immune cell atlas of human neuroblastoma. *Cell Rep Med* 2022;3:100657.
31 Zhang W, Yu Y, Hertwig F, *et al*. Comparison of RNA-seq and microarray-based models for clinical endpoint prediction. *Genome Biol* 2015;16:133.
32 Heath WR, Kato Y, Steiner TM, *et al*. Antigen presentation by dendritic cells for B cell activation. *Curr Opin Immunol* 2019;58:44–52.
33 Maddur MS, Sharma M, Hegde P, *et al*. Human B cells induce dendritic cell maturation and favour Th2 polarization by inducing OX-40 ligand. *Nat Commun* 2014;5:4092.
34 Pitzalis C, Jones GW, Bombardieri M, *et al*. Ectopic lymphoid-like structures in infection, cancer and autoimmunity. *Nat Rev Immunol* 2014;14:447–62.
35 Petroni G, Pillozzi S, Antonuzzo L. Exploiting Tertiary Lymphoid Structures to Stimulate Antitumor Immunity and Improve Immunotherapy Efficacy. *Cancer Res* 2024;84:1199–209.
36 Greenwald NF, Miller G, Moen E, *et al*. Whole-cell segmentation of tissue images with human-level performance using large-scale data annotation and deep learning. *Nat Biotechnol* 2022;40:555–65.
37 Bishayee K, Habib K, Sadra A, *et al*. Targeting the Difficult-to-Drug CD71 and MYCN with Gambogic Acid and Vorinostat in a Class of Neuroblastomas. *Cell Physiol Biochem* 2019;53:258–80.
38 Skertich NJ, Chu F, Tarhoni IAM, *et al*. Expression of Immunomodulatory Checkpoint Molecules in Drug-Resistant Neuroblastoma: An Exploratory Study. *Cancers (Basel)* 2022;14:751.
39 Larkin RM, Lopez DC, Robbins YL, *et al*. Augmentation of tumor expression of HLA-DR, CXCL9, and CXCL10 may improve olfactory neuroblastoma immunotherapeutic responses. *J Transl Med* 2024;22:524.
40 Mirlekar B, Wang Y, Li S, *et al*. Balance between immunoregulatory B cells and plasma cells drives pancreatic tumor immunity. *Cell Rep Med* 2022;3:100744.
41 Suan D, Kräutler NJ, Maag JLV, *et al*. CCR6 Defines Memory B Cell Precursors in Mouse and Human Germinal Centers, Revealing Light-Zone Location and Predominant Low Antigen Affinity. *Immunity* 2017;47:1142–53.
42 Lu J, Wu J, Mao L, *et al*. Revisiting PD-1/PD-L pathway in T and B cell response: Beyond immunosuppression. *Cytokine Growth Factor Rev* 2022;67:58–65.
43 Santegoets SJ, Duurland CL, Jordanova ES, *et al*. Tbet-positive regulatory T cells accumulate in oropharyngeal cancers with ongoing tumor-specific type 1 T cell responses. *J Immunother Cancer* 2019;7:14.
44 Cabrita R, Lauss M, Sanna A, *et al*. Tertiary lymphoid structures improve immunotherapy and survival in melanoma. *Nature New Biol* 2020;577:561–5.
45 Wienke J, Visser LL, Kholosy WM, *et al*. Integrative analysis of neuroblastoma by single-cell RNA sequencing identifies the NECTIN2-TIGIT axis as a target for immunotherapy. *Cancer Cell* 2024;42:283–300.
46 Meylan M, Petitprez F, Becht E, *et al*. Tertiary lymphoid structures generate and propagate anti-tumor antibody-producing plasma cells in renal cell cancer. *Immunity* 2022;55:527–41.
47 Patil NS, Nabet BY, Müller S, *et al*. Intratumoral plasma cells predict outcomes to PD-L1 blockade in non-small cell lung cancer. *Cancer Cell* 2022;40:289–300.
48 Bouloudani T, Pupier G, Sautès-Fridman C, *et al*. B cells are major players in cancer immunity. *Immunol Lett* 2025;276:107064.
49 Zhao L, Jin S, Wang S, *et al*. Tertiary lymphoid structures in diseases: immune mechanisms and therapeutic advances. *Signal Transduct Target Ther* 2024;9:225.
50 Xu W, Lu J, Liu W-R, *et al*. Heterogeneity in tertiary lymphoid structures predicts distinct prognosis and immune microenvironment characterizations of clear cell renal cell carcinoma. *J Immunother Cancer* 2023;11:e006667.
51 Hugaboom MB, Wirth LV, Street K, *et al*. Presence of Tertiary Lymphoid Structures and Exhausted Tissue-Resident T Cells Determines Clinical Response to PD-1 Blockade in Renal Cell Carcinoma. *Cancer Discov* 2025;15:948–68.
52 Elgueta R, Marks E, Nowak E, *et al*. CCR6-dependent positioning of memory B cells is essential for their ability to mount a recall response to antigen. *J Immunol* 2015;194:505–13.
53 Gu-Trantien C, Loi S, Garaud S, *et al*. follicular helper T cell infiltration predicts breast cancer survival. *J Clin Invest* 2013;123:2873–92.
54 Xiao Z, Mayer AT, Nobashi TW, *et al*. ICOS Is an Indicator of T-cell-Mediated Response to Cancer Immunotherapy. *Cancer Res* 2020;80:3023–32.
55 Garaud S, Dieu-Nosjean MC, Willard-Gallo K. T follicular helper and B cell crosstalk in tertiary lymphoid structures and cancer immunotherapy. *Nat Commun* 2022;13:2259.
56 Kalergis AM, Ravetch JV. Inducing tumor immunity through the selective engagement of activating Fcgamma receptors on dendritic cells. *J Exp Med* 2002;195:1653–9.
57 Melaiu O, Fruci D. IMC data - Mapping B cells and the immune landscape of tertiary lymphoid structures reveals their clinical impact in neuroblastoma. *Zenodo* 2025.